Impact of Handling Qualities on Motor Sizing for Multirotor Aircraft with Urban Air Mobility Missions

Shannah Withrow-Maser
shannah.n.withrow@nasa.gov
Ames Research Center
Moffett Field, CA, USA

Carlos Malpica
carlos.a.malpica@nasa.gov
Ames Research Center
Moffett Field, CA, USA

Keiko Nagami
keiko.nagami@nasa.gov
Ames Research Center
Moffett Field, CA, USA

ABSTRACT

Control models of three NASA Urban Air Mobility (UAM) reference vehicles (the quadrotor, octocopter, and Lift+Cruise (LPC)) were created and compared to determine the effect of rotor number and disk loading on control margin and design. The heave and yaw axes demand more actuator usage than the roll and pitch axes. Between heave and yaw, heave was the more demanding of the two because of the dependence of heave on the engine speed controller (ESC). When the feedback gains for all three vehicles were optimized to Level 1 handling qualities (HQs) specifications using CONDUIT, the ESC for the octocopter was the most stable and had the highest rise time (time for the rotor to respond to an input), while the LPC ESC was the least stable and had the smallest rise time. Rise time corresponds to the time required for rotor response. When actuator usage was translated to current margin, torque margin, and power margin, heave was the most demanding axis, followed by yaw, roll, and then pitch for all three vehicles. The results emphasize the importance of an accurate motor model within the control system architecture.

NOTATION

A_{ref}	Reference area (ft^2)
A_{rms}	Actuator (motor current) usage metric
B	Motor friction and viscous losses coefficient
c	Torque SI unit conversion constant (0.7374 lb-ft/Nm)
C_{l_α}	Lift curve slope
DL	Disk loading (lb/ft^2)
f_d	Drive system inertia factor
FM	Figure of merit
g	Gravitational acceleration (ft/s^2)
I	Current (A)
I_{xx}	Moment of inertia, x-axis (slug ft^2)
I_{yy}	Moment of inertia, y-axis (slug ft^2)
I_{zz}	Moment of inertia, z-axis (slug ft^2)
I_R	Main rotor rotational moment of inertia (slug ft^2)
I_{P_i}	Total propulsion system rotational moment of inertia (slug ft^2)
J	Drive system rotational moment of inertia (slug ft^2)
K_e	Motor back-EMF constant (Vs)
K_i	Integral ESC feedback gain (V/rad)
K_m	Motor torque constant (lb-ft/A), $K_m = cK_e$
K_p	Proportional ESC feedback gain (Vs/rad)
m	Mass (slug)
N_r	Yaw damping term
N_R	Number of rotors
P	Power (hp)
Q	Torque (lb-ft)
Q_A	Rotor aerodynamic torque (lb-ft)
Q_S	Rotor shaft torque (lb-ft)
p	Roll rate (rad/s)
q	Pitch rate (rad/s)
r	Yaw rate (rad/s)
r_g	Drive system gear ratio
r_i	Direction of rotation of i-th rotor
R	Rotor radius (ft)
R_a	Motor armature resistance (Ω)
s	Laplace domain variable (rad/s)
t	Time (s)
t_r	Rise time (s)
T	Thrust (lb)
u	Body axis longitudinal velocity (ft/s)
v	Body axis lateral velocity (ft/s)
V	Voltage (V)
V_i	Motor armature voltage input (V)
w	Body axis heave rate (ft/s)
ΔI_{max}	Maximum current limit margin (A)
ϕ	Roll angle (deg)
θ	Pitch angle (deg)

Presented at the Vertical Flight Society's 77th Annual Forum & Technology Display, Virtual, May 10-14, 2021.

ψ	Yaw angle (deg)
$\Delta\Omega_{max}$	Rotor speed change for ΔI_{max} (rad/s)
η	Motor efficiency factor
λ	Inflow ratio
λ_i	Induced inflow ratio
φ_I	Nominal motor voltage-to-current design ratio
ω	Motor speed (rad/s)
ω_n	Natural Frequency (rad/s)
v_i	Induced velocity (ft/s)
κ	Induced power loss coefficient
ζ	Damping ratio
σ	Rotor solidity
Ω	Main rotor speed (rad/s)
τ	Motor shaft torque (lb-ft)
ρ	Air density (slug/ft^3)

INTRODUCTION

Multirotor configurations are being considered for many new and current Urban Air Mobility (UAM) concepts. Electric VTOL News reports that there are at least 113 multirotor UAM concepts as of April 2021 (Ref. 1). This configuration is especially popular for all-electric, variable rotor speed-controlled vehicles in order to generate sufficient lift. While multirotor configurations are common for smaller aircraft, the handling qualities performance of configurations scaled for UAM application is still under investigation. Previously, the authors (Ref. 2) were able to stabilize the roll axis for a UAM-sized quadrotor, hexacopter, and octocopter but only with significant power draw. This work will expand that previous study and add an additional vehicle configuration (the Lift+Cruise (LPC)). In variable rotor speed-controlled vehicles, the propulsion system is directly in the path of the control system, which means the stability and control of the vehicle must be well understood to determine power requirements and the related overall weight of the vehicle. The objective of this work is twofold: 1) Determine the power requirements associated with the potentially more demanding heave and yaw axes and 2) Compare the NASA quadrotor, octocopter, and LPC concept vehicles in the heave and yaw axes to investigate how number of rotors and disk loading affects the required control margins. The quadrotor and octocopter will be compared to investigate effect of number of rotors and the octocopter and LPC configuration will be compared to investigate the effect of disk loading. Additionally, the effect of rotor design parameters on the control derivatives and design implication is discussed on the basis of fundamental blade element momentum theory.

BACKGROUND

Previous work shows that rotor size and disk loading have an effect on controllability and can influence the number of rotors chosen for a UAM multirotor concept (Ref. 5 and 6). In Schuet et al, (Ref. 3) controllability restrictions due to limited available power were discussed. Malpica and Withrow-Maser (Ref. 4) showed that quadrotors with variable-pitch rotors could be designed to meet Level 1 HQ specifications and that drive system limits in quadrotors using variable-speed rotors prevented the stabilization of pitch and roll with the provided assumptions within adequate margins. Withrow-Maser and Malpica (Ref. 2) found a solution for the quadrotor and extended the analysis of the speed-controlled design to the engine speed controller (ESC) design (with adequate design) of a hexacopter and octocopter sized for the same UAM mission by looking at the trade of disturbance rejection and actuator (engine) usage in the roll axis.

Simultaneously, Walter et al. (Ref. 5) investigated UAM quadrotors with increasing rotor size and determined that heave and yaw were the limiting axes. Assuming this trend holds for other multirotors in the same class, an independent assessment of these trades is warranted, and it is desirable to characterize the NASA reference quadrotor in these axes and expand it to other multirotor configuration such as the octocopter and LPC concept vehicles. Additionally, Bahr et al. (Ref. 6) also described variations of multirotor UAM concepts with equal gross weights and disk area in hover and determined motor weight required for controllability as a percentage of total weight. This work will be discussed in context of the NASA vehicles.

OBSERVATIONS FROM THEORY

Heave and Yaw Dynamics

In order to investigate the effect of the key parameters that govern heave and yaw control effectiveness it is useful to formulate the equations of motion in a simplified representation. Retaining explicitly only the rotor thrust and torque contributions, assuming quasi-steady inflow dynamics, and assuming body-frame coincident with the principal axes, the vehicle and rotor equations of motion in hover can be represented by:

$$\dot{u} = \frac{X(u)}{m} - \frac{1}{m}\sum_{i=1}^{N_R} T_i \alpha_i - g\sin\theta \tag{1}$$

$$\dot{v} = \frac{Y(v)}{m} + \frac{1}{m}\sum_{i=1}^{N_R} T_i \beta_i + g\sin\phi\cos\theta \tag{2}$$

$$\dot{w} = -\frac{1}{m}\sum_{i=1}^{N_R} T_i + g\cos\phi\cos\theta \tag{3}$$

$$\dot{p} = \frac{1}{I_{xx}} \sum_{i=1}^{N_R} \left[Q_{S_i} \alpha_i r_i - (y_i + z_i \beta_i) T_i \right] \tag{4}$$

$$\dot{q} = -\frac{1}{I_{yy}} \sum_{i=1}^{N_R} \left[Q_{S_i} \beta_i r_i - (x_i - z_i \alpha_i) T_i \right] \tag{5}$$

$$\dot{r} = \frac{N(r)}{I_{zz}} + \frac{1}{I_{zz}} \sum_{i=1}^{N_R} \left[Q_{S_i} r_i + (x_i \beta_i + y_i \alpha_i) T_i \right] \tag{6}$$

and

$$\dot{\Omega}_i - r_i \dot{r} = \frac{Q_{A_i}}{I_{R_i}} + \frac{Q_{S_i}}{I_{R_i}} \tag{7}$$

for $i = 1, 2 \ldots N_R$ (N_R being the number of rotors). Here, T_i and Q_{S_i} are the thrust and shaft torque of the i-th rotor, which are transmitted to the airframe. The location of each rotor hub is defined, in body-axis coordinates, by x_i, y_i and z_i. The rotor shafts may be tilted longitudinally (α_i positive aft) or laterally (β_i positive to the right). Quasi-steady rotor flapping contributions to the rotor drag and other airframe components are accounted for in $X(u)$, $Y(v)$ and $N(r)$. The convention chosen here for a positive torque is such that it causes the rotor to accelerate, or increase speed, in its normal direction of rotation. Thus r_i is chosen to account for the direction of rotation of the rotor (1 for counter-clockwise, –1 for clockwise rotation). Hence, a positive shaft torque acting on a counter-clockwise rotating main-rotor results in a positive yaw moment reaction on the fuselage (in the body frame).

Considering the linear equations of motion for small-perturbation heave, yaw, and rotor speed and assuming no shaft tilt with respect to the body frame z-axis would lead to:

$$\dot{w} = -\frac{1}{m} \sum_{i=1}^{N_R} \frac{\partial T_i}{\partial w} w - \frac{1}{m} \sum_{i=1}^{N_R} \frac{\partial T_i}{\partial \Omega_i} \Omega_i \tag{8}$$

$$\dot{r} = \frac{N_r}{I_{zz}} r + \frac{1}{I_{zz}} \sum_{i=1}^{N_R} Q_{S_i} r_i \tag{9}$$

$$\dot{\Omega}_i = \frac{1}{I_{R_i}} \frac{\partial Q_{A_i}}{\partial w} w + \left(\frac{1}{I_{R_i}} \frac{\partial Q_{A_i}}{\partial r} + r_i \frac{N_r}{I_{zz}} \right) r + \frac{1}{I_{R_i}} \frac{\partial Q_{A_i}}{\partial \Omega_i} \Omega_i + \frac{Q_{S_i}}{I_{R_i}} \tag{10}$$

for $i = 1, 2 \cdots N_R$.

Further simplifying assumptions include neglecting rotor translational lift from the yaw motion (small in magnitude) and rotor aerodynamic interactions.

Inspection of the reduced heave equation of motion suggests that control depends primarily on the rotor speed. The required time constant of the rotor response is a question of fundamental importance to understanding the overall responsiveness of the vehicle. Interestingly, because of the direct torque reactions on the airframe, yaw torque can be applied almost instantaneously, suggesting potentially higher control responsiveness. Torque that can be applied to the rotor from the electric motors is:

$$Q_{S_i} = \frac{r_g K_m}{R_a} V_i - \frac{r_g^2 K_e K_m}{R_a} \Omega_i - J r_g^2 \dot{\Omega}_i \tag{11}$$

for $i = 1, 2 \cdots N_R$.

Therefore, application of a voltage command to the motor armature circuit results in a nearly instantaneous torque response of the open loop. As speed increases the back-EMF voltage drop will reduce the effectiveness of the voltage command.

$$\dot{r} = \frac{N_r}{I_{zz}} r - \frac{1}{I_{zz}} \sum_{i=1}^{N_R} \frac{r_g^2 K_e K_m}{R_a} r_i \Omega_i + \frac{1}{I_{zz}} \sum_{i=1}^{N_R} \frac{r_g K_m}{R_a} r_i V_i \tag{12}$$

$$\dot{\Omega}_i = \frac{1}{I_{P_i}} \frac{\partial Q_{A_i}}{\partial w} w + \left(\frac{1}{I_{P_i}} \frac{\partial Q_{A_i}}{\partial r} + r_i \frac{N_r}{I_{zz}} \right) r + \frac{1}{I_{P_i}} \left(\frac{\partial Q_{A_i}}{\partial \Omega_i} - \frac{r_g^2 K_e K_m}{R_a} \right) \Omega_i + \frac{1}{I_{P_i}} \frac{r_g K_m}{R_a} V_i \tag{13}$$

for $i = 1, 2 \cdots N_R$. By virtue of the back-EMF, the coupling of the electric propulsion system to the bare-airframe introduces additional linear terms of the rotor speed. In particular, the back-EMF was argued in Ref. 4 to contribute

to the pole of the rotor speed equations of motion. Accounting for the ESC dynamics and both collective (Ω_{col}) and differential (pedal) (Ω_{ped}) rotor speed command control allocation schemes, the equations can be expressed as:

$$\dot{w} = -\frac{1}{m}\sum_{i=1}^{N_R}\frac{\partial T_i}{\partial w}w - \frac{1}{m}\sum_{i=1}^{N_R}\frac{\partial T_i}{\partial \Omega_i}\tau_\Omega(t) * \Omega_{col}(t) \quad (14)$$

$$\dot{r} = \frac{N_r}{I_{zz}}r + \frac{1}{I_{zz}}\sum_{i=1}^{N_R}\frac{r_g K_m}{R_a}(\tau_V(t) - r_g K_e \tau_\Omega(t)) * \Omega_{ped}(t) \quad (15)$$

where $\tau_\Omega(t)$ and $\tau_V(t)$ are the closed-loop ESC speed and voltage impulse response functions, respectively. Formulated in this fashion, Eqs. 14 and 15 allow the examination of the heave and yaw controllability, in an open-loop sense. Attention will be focused on the qualification of the key derivatives and ESC performance from a theoretical point of view.

Rotor Thrust and Torque Derivatives

From blade element momentum theory, streamlined expressions can be derived for the key thrust and torque derivatives for individual rotors. Recognizing the limitations espoused in References 7-9, the classical quasi-static equation for the uncoupled vertical motion of the helicopter provides a simple expression for the heave damping:

$$\frac{\partial T}{\partial w} = \frac{\rho\sigma C_{l_\alpha} A_{ref} V_{tip}}{8\left(1 + \frac{\sigma C_{l_\alpha}}{16\lambda_i}\right)} \quad (16)$$

A reasonable approximation for the rotor thrust derivative with respect to rotor speed can be found to be:

$$\frac{\partial T}{\partial \Omega} = \sigma C_{l_\alpha}\rho A_{ref}\left(\frac{\theta_{75}}{3} - \frac{\lambda}{2}\right)R^2\Omega \quad (17)$$

In terms of the rotor thrust, $T \sim \Omega^2$ for fixed pitch, therefore,

$$\frac{\partial T}{\partial \Omega} = \frac{2T}{\Omega} \quad (18)$$

or,

$$\frac{\partial T}{\partial \Omega} = \frac{2T}{V_{tip}}R \quad (19)$$

Similar analytical expressions for rotor torque derivatives are, thus, proposed:

$$\frac{\partial Q_A}{\partial w} = \frac{3\kappa R}{2V_{tip}}\left[v_i\frac{\partial T}{\partial w} + \frac{T}{3}\right] - \frac{TR}{V_{tip}} - \frac{\frac{\partial P_0}{\partial \lambda}\cdot\frac{R}{V_{tip}^2}}{2\left(1 + \frac{\sigma C_{l_\alpha}}{16\lambda_i}\right)} \quad (20)$$

And $Q \sim \Omega^2$ for fixed pitch, therefore

$$\frac{\partial Q_A}{\partial \Omega} = \frac{2P}{\Omega^2} \quad (21)$$

or,

$$\frac{\partial Q_A}{\partial \Omega} = \frac{2P}{V_{tip}^2}R^2 \quad (22)$$

From Eq. 19, it is seen that rotor thrust control derivatives (considering rotor speed as the control input) depend fundamentally on rotor thrust, rotor size, and tip speed. In hover, thrust depends on the weight, and tip speed is nominally set to account for noise and compressibility considerations. Therefore, the control derivative is fundamentally and directly related to the rotor size. A similar relationship is observed from the rotor torque derivative, in Eq. 22, where rotor power will depend on parameters that contribute to the induced and profile power losses.

It is interesting to note the implications of vehicle design parameters on the thrust and torque derivatives with respect to rotor speed, and thus on the effectiveness of RPM control in hover. Eqs. 19 and 22 can be expressed in terms of more basic rotor design parameters. For instance:

$$\frac{\partial T}{\partial \Omega} = 2\pi R^3 \cdot \frac{DL}{V_{tip}} \quad (23)$$

and

$$\frac{\partial Q_A}{\partial \Omega} = \frac{2\pi R^4}{\sqrt{2\rho}} \cdot \frac{\sqrt{DL^3}}{V_{tip}^2 FM} \quad (24)$$

show the relationships to disk loading, tip speed, and for the torque derivative, figure of merit.

For best hover performance, rotorcraft design usually strives to maximize figure of merit and to minimize the disk loading as much as practical. This last point is important because this goal will require a large rotor and other design constraints will become relevant. Eqn. 24 implies that thrust and torque derivatives would maintain a directly proportional relationship with R (as previously shown in Eqs. 19 and 22) because the disk loading for a given thrust (fraction of the weight) is inversely proportional to the disk area (and hence to R^2). Therefore, the goal of minimizing the disk loading (and maximizing the figure of merit) also achieves increased thrust control power and rotor speed damping per thruster. These benefits of larger rotors need to be counterbalanced with the negative aspects, such as the increased rotor moment of inertia.

Table 1 compares three different rotorcraft configurations (Figure 1), of approximately comparable gross weight, spanning the design space in terms of number of rotors and disk loading, both of which have a determining effect on the rotor size. The quadrotor and octocopter, having been sized to the same disk loading can be compared in this respect. Comparison between the aircraft is complicated slightly by the differences in the hover tip speed to trim the vehicle, reflecting the rotor pitch setting. However, even after accounting for the number of rotors and the tip speed, and considering it is a heavier configuration, the total thrust control derivative for the octocopter is found to be only marginally smaller. Where the octocopter may have a marginal advantage is in the slightly higher heave damping as seen in Table 1. The quadrotor and octocopter are sized for fixed disk loading with rotor radius fallout, while the LPC aircraft has radius fixed and disk loading fallout. The effect of the higher disk loading and smaller rotor size on the thrust control derivative is evident between the octocopter and LPC, both having eight rotors, with the LPC derivatives providing significantly lower thrust control power.

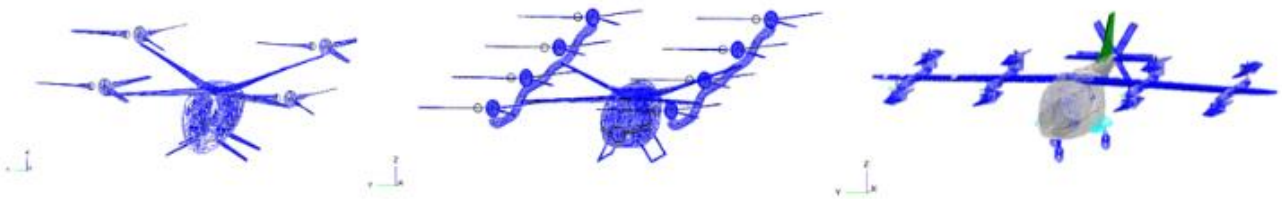

Figure 1. OpenVSP model showing rotor configuration: Quadrotor, Octocopter, and LPC.

Table 1. Effect of rotorcraft design parameters on key thrust and torque derivatives.

Parameter	Units	Quadrotor	Octocopter	Lift+Cruise
Number of rotors	–	4	8	8
Design disk loading	lb/ft^2	3	3	–
Design tip speed	ft/s	550	550	550
Density	slug/ft^3	0.0020	0.0020	0.0020
Radius	ft	12.3	9.5	5
Solidity	–	0.0555	0.0555	0.1563
Rotor area (total)	ft^2	1905.5	2282.3	628.3
Design Gross Weight	lb	5716.4	6846.8	5903.0
Average disk loading (hover)	lb/ft^2	3.00	3.00	9.44
Average tip speed (hover)	ft/s	492.4	549.8	533.4
Mass	slug	177.5	212.6	183.3
Rotor moment of inertia	slug·ft^2	202.6	66.7	21.4
Average rotor power (hover)	hp	91.3	57.1	93.1
Average rotor torque (hover)	lb·ft	1254.3	544.2	480.1
Average $\partial T/\partial \Omega$	lb·s/rad	71.43	29.66	13.90
Average $\partial Q_A/\partial \Omega$	lb·ft s/rad	–62.69	–18.86	–9.00
Average $\partial T/\partial w$	lb·s/ft	14.37	9.06	6.33
Average $\partial Q_A/\partial$w	lb·s	5.23	2.20	5.55

Bare Airframe Source and Integration

NDARC was used to size the three, six-passenger vehicles to the same mission (Ref. 10) with two segments of 75 nautical miles, 30 seconds of hover time each, and 20 minutes of cruise reserve. SIMPLI-FLYD (Ref. 11) was then utilized to generate the bare airframe model which was imported into the CONDUIT (Ref. 12) block diagram. For the CONDUIT set up, a model following control system architecture was followed with an electric motor and speed controller integrated into the block diagram as described in Ref. 2.

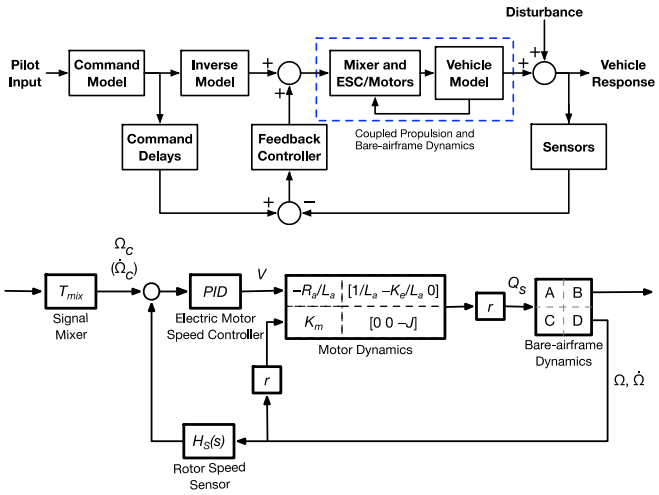

Figure 2: Block diagram of control system architecture including motor dynamics.

Control Effectiveness

Aircraft heave damping and control derivatives, as well as rotor torque derivatives, associated with these simple analytical representations are compared to higher-order perturbation model values from the SIMPLI-FLYD (Ref. 11) in Table 2. Overall, there was very good agreement between the two sets of parameters, with the exception of the torque derivative due to heave rate, but these are typically small and had little impact on the performance of the controller. Also included in Table 2 are the perturbation model values for the yaw damping derivatives, N_r. Analytical representations of the yaw damping, similar to the ones presented above were beyond the scope of the current discussion, but it is illustrative to identify the main sources of the yaw damping from the model. For the quadrotor and octocopter, the dominant contribution to the yaw damping is from the main rotors. A significant portion of this is associated with the quasi-steady rotor flap response of the articulated or soft hingeless flapping rotors (1.03/rev flap frequency) to a yaw rate perturbation. This effect is less pronounced for the LPC, with stiffer hingeless rotors (1.25/rev flap frequency), but additional contributions from the pusher propeller wing, and empennage need to be taken into consideration. These are strongly dependent on the aerodynamic interactions with the rotor wakes and are thus non-trivial to estimate and a source of significant uncertainty. In the absence of rotor wake induced flow impinging on the airframe components, contributions to the yaw damping in hover of these components should be negligible because of the low dynamic pressures.

Table 2. Key heave and rotor response derivatives for quadrotor.

		Quadrotor		Octocopter		Lift+Cruise	
Parameter	**Units**	**Estimate**	**Model**	**Estimate**	**Model**	**Estimate**	**Model***
$\frac{\partial Z}{\partial \Omega_0}\frac{1}{m}$	ft/s	–1.610	–1.583	–1.116	–1.020	–0.607	–0.673
$\frac{\partial Q_A}{\partial \Omega}\frac{1}{I_R}$	1/s	–0.309	–0.317	–0.283	–0.293	–0.420	–0.446
$\frac{\partial Z}{\partial w}\frac{1}{m}$	1/s	–0.324	–0.327	–0.341	–0.373	–0.276	– 0.283
$\frac{\partial Q_A}{\partial w}\frac{1}{I_R}$	rad/ft·s	0.026	0.003	0.033	0.006	0.260	–0.064
$\frac{\partial N}{\partial r}\frac{1}{I_{zz}}$	1/s	—	–0.226	—	–0.150	—	–0.080

* Only direct contribution of the lifting rotors listed, without effect of aerodynamic interactions

The heave damping derivatives from Table 2 would suggest the slowest open-loop response (in the case of the LPC) would exhibit a time constant of 4 s, assuming instantaneous thrust were delivered by the rotors. This in principle meets Level 1 requirements according to ADS-33, but whether this response bandwidth is sufficient to meet the ostensibly higher precision required by the UAM mission is still undetermined. Regardless, taking the five second time constant requirement, additional time constants associated with the rotor speed response would need to be limited to about one second.

Engine Speed Controller (ESC)

Assessment of control effectiveness has a clear dependence on the engine speed controller (ESC). Accounting for the moment of inertia contribution of the motor and other high-speed transmission components, and neglecting, for now, heave and yaw dynamics (which would be seen by the ESC as perturbations), the closed-loop transfer functions of the ESC compensator take the form:

$$\frac{V_a(s)}{\Omega_{cmd}(s)} = \left(K_p + \frac{K_i}{s}\right)\left(1 - \frac{\Omega(s)}{\Omega_{cmd}(s)}\right) \tag{25}$$

and

$$\frac{\Omega(s)}{\Omega_{cmd}(s)} = \frac{\frac{cK_e r}{I_P R_a}K_p s + \frac{cK_e r}{I_P R_a}K_i}{s^2 + \left(p_R + \frac{cK_e r}{I_P R_a}K_p\right)s + \frac{cK_e r}{I_P R_a}K_i} \tag{26}$$

where,

$$p_R = \frac{cK_e^2 r^2}{I_P R_a} - \frac{1}{I_P}\frac{\partial Q_A}{\partial \Omega}$$

is the bare-airframe coupled rotor-engine dynamic pole. Note that Eq. (26) can be expressed in form

$$\frac{\Omega(s)}{\Omega_{cmd}(s)} = \frac{\frac{\omega_n}{\alpha\zeta}s + \omega_n^2}{s^2 + 2\zeta\omega_n s + \omega_n^2} \tag{27}$$

where,

$$\omega_n^2 = \frac{cK_e r}{I_P R_a}K_i \tag{28}$$

$$2\zeta\omega_n = \frac{cK_e^2 r^2}{I_P R_a} - \frac{1}{I_P}\frac{\partial Q_A}{\partial \Omega} + \frac{cK_e r}{I_P R_a}K_p \tag{29}$$

and

$$\frac{\omega_n}{\alpha\zeta} = \frac{cK_e r}{(I_r + Jr^2)R_a}K_p \tag{30}$$

For a system of the form of Eqn. 27, where the response is the superposition of the response of a classical second order system and a term proportional to the rate, the zero $s = -\alpha\zeta\omega_n$ can have a very strong impact on the rise time and peak magnitude (Ref. 13). To minimize the effect of this zero, it is advisable to place it far away from the poles, and thus α needs to be made large (e.g., $\alpha > 4$).

For a given a motor, Eqn. 28 suggests natural frequency for a given propulsion system design depends solely on integral ESC compensation K_i. Considering Eqn. 29, the proportional gain K_p would therefore be the primary means of injecting damping into the response. It is noted that this equation could potentially yield negative solutions for gain K_p, depending on the desired dynamic response. The system of equations defined by Eqns. 28 and 29, with K_i and K_p as the only unknowns, is overdetermined and a unique solution cannot be guaranteed. The position of the aforementioned transfer function zero is therefore dependent on the feedback gains. Dividing Eq. 28 by 30, however, it is straightforward to show that the transfer function zero depends solely on the ratio of the integral and proportional ESC compensation:

$$\alpha\zeta\omega_n = \frac{K_i}{K_p} \tag{31}$$

Time domain characterizations of the dynamic response of the ESC include the rise time t_r (the time required for the response to rise from 10% to 90% of its final value) and the peak overshoot M_p (the deviation of the response at peak time from the final value of response). The step response rise time correlates with the damped frequency of the system, and indirectly to the bandwidth. The peak overshoot provides an estimate of the damping ratio of the ESC. There are no clear guidelines as to what values of the rise time and peak overshoot are required for good vehicle response, but good engineering practice would dictate lightly damped flight control components should be avoided to avoid stability margin degradation. Figure 3 shows the relationships between the time domain dynamics characterization of the ESC response and the pole damping ratio and natural frequency. Figure 4 illustrates the functional relationship between the two feedback gains and the ESC rise time and peak overshoot characteristics. Clearly, even for a well-damped response, with less than 1% overshoot, there is still a wide design space in terms of the rise time of response.

Frequency and step responses in Figure 5 and Figure 6 illustrate the potential effect of the ESC on the open-loop heave and yaw response of a simple first order representation of the quadrotor modeled after the derivatives of Table 2. The ESC was configured by selecting proportional and integral

gains from Figure 4 to provide a rise time of 0.7 s and less than 1% overshoot. In Ref. 2 it was determined, based on roll stabilization of the quadrotor model, that ESC response bandwidth should be somewhere in the neighborhood of 0.4–0.8 s. The ESC is shown to introduce significant phase delay in the heave response (effectively turning it into a second-order system) and significant phase lead into the yaw response because of the direct application of torques. Overall control power is also seen to be satisfactory. The unit step input of Figure 5 was of a magnitude of 1 rad/s, or roughly 10 RPM. The quadrotor can be seen to achieve nearly 300 ft/min in response to this collective rotor speed command and almost 300 deg/s in response to a differential rotor speed command. Comparatively, the octocopter in Figure 7 demonstrates about 180 ft/min and the LPC only about 120 ft/min for the same command size.

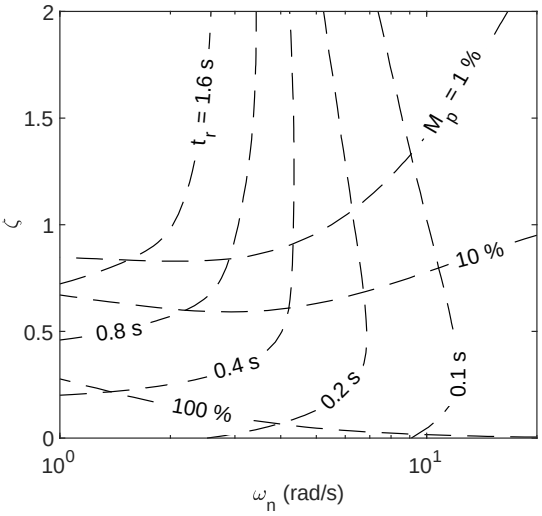

Figure 3. Damping ratio vs natural frequency.

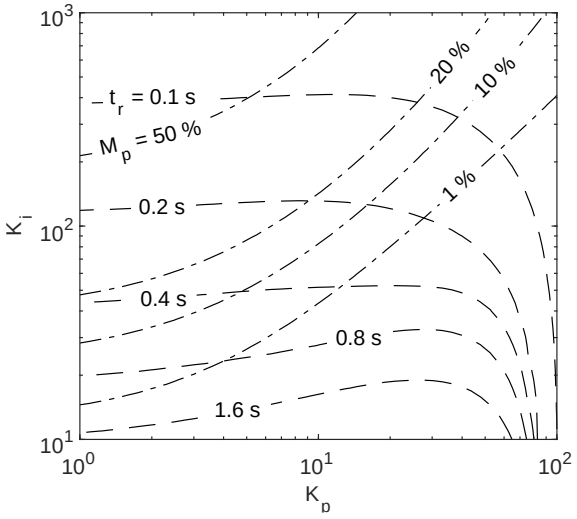

Figure 4. Gain map.

While this discussion illustrates some of the competing requirements for the ESC feedback gains K_p and K_i, results are to some extent academic. The discussion focuses on the ESC dynamic response in isolation, without consideration for the stability of the feedback-loop when other dynamics, including the electrical inductance, are present. The present discussion also pays little attention to the potential exceedance of any propulsion torque and/or power limits, nor the motor usage. More generally, the problem needs to consider the overall aircraft feedback stabilization requirements, and specific rise time to achieve these is unknown. In practice, feedback control would be used to quicken the response, so considerations need to turn to the available stability margins, etc. Modern control laws will be concerned with enforcing specific disturbance rejection and agility requirements, important considerations for the UAM mission. However, such considerations are beyond the simple quasi-steady model presented.

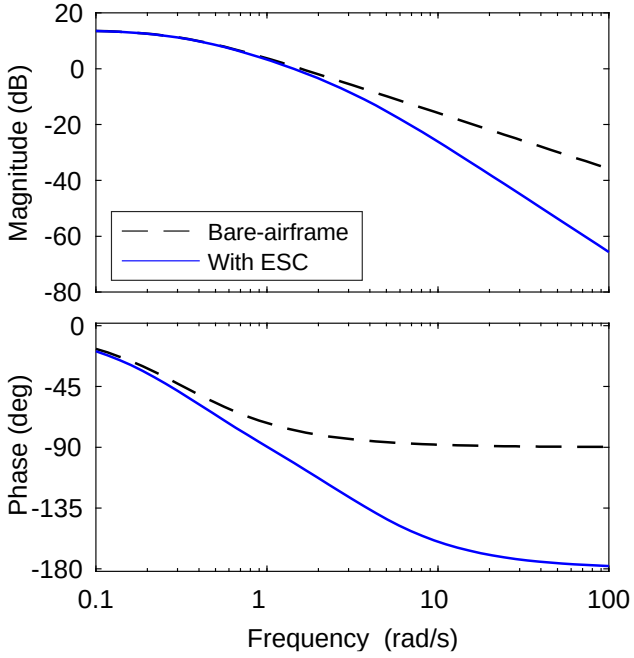

(a) Heave

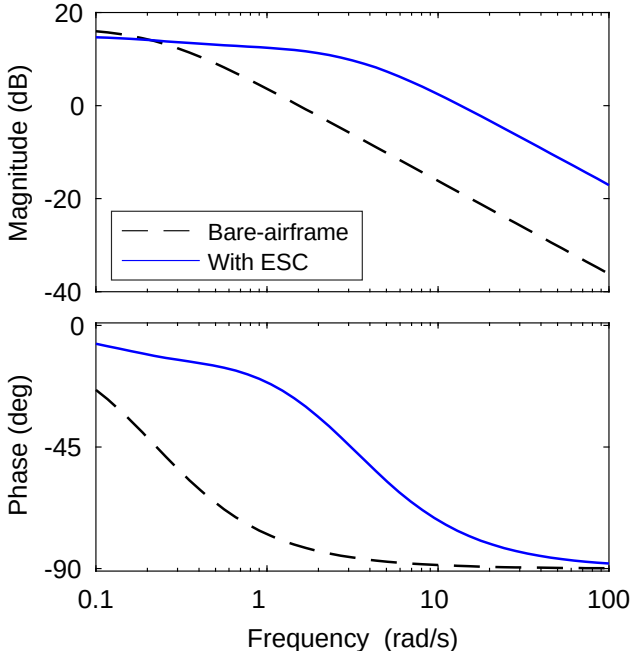

(b) Yaw

Figure 5. Open-loop frequency response to commanded rotor speed.

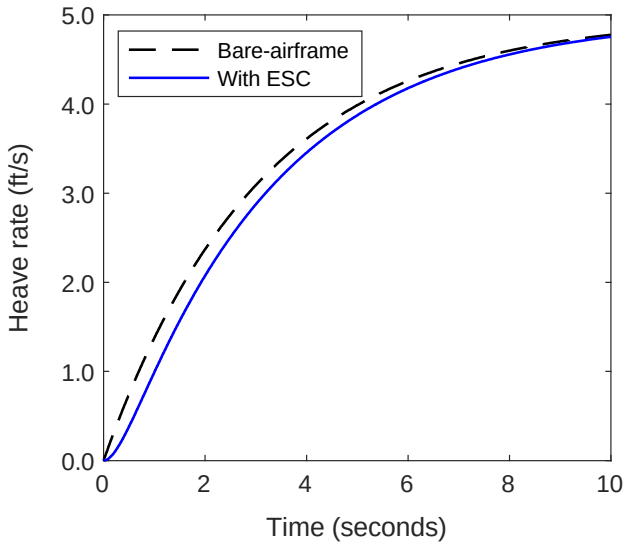

(a) Heave

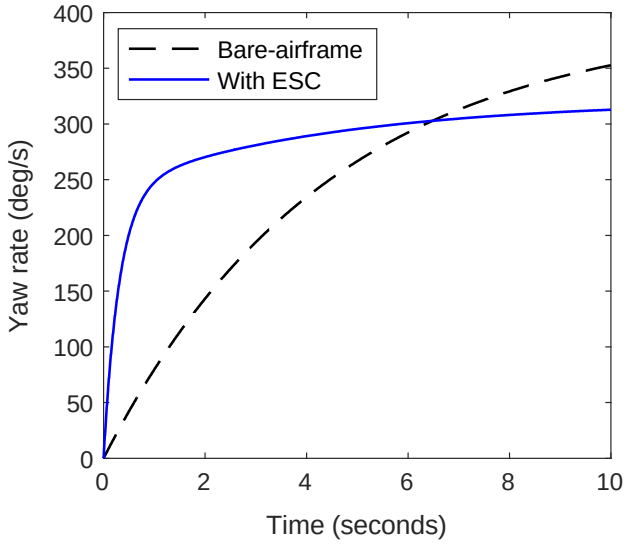

(b) Yaw

Figure 6. Open-loop step response to commanded rotor speed.

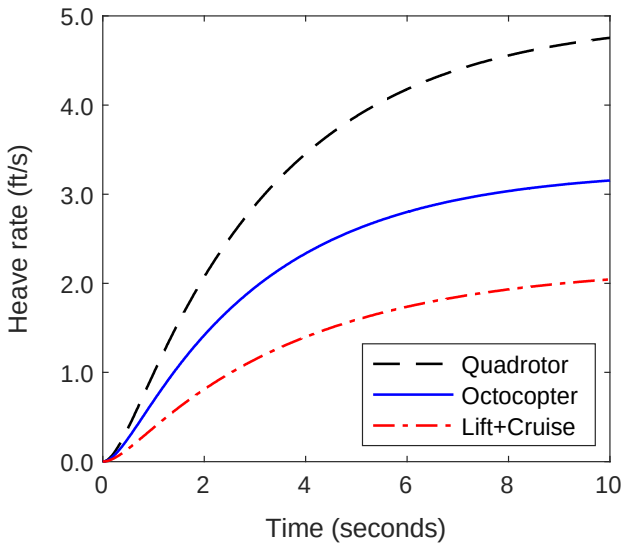

Figure 7. Comparison of open-loop heave response for the Quadrotor, Octocopter and LPC configurations based on simple first-order model.

After exhausting the limits of the simple quasi-steady model described above, the problem was further explored considering the multi-objective control system design and optimization for higher-order models of the vehicle designs.

MULTI-OBJECTIVE FUNCTION CONTROL OPTIMIZATION

While the previous discussion served to illustrate some of the fundamental challenges of using rotor speed for control in connection with the vehicle design parameters, a more complete analysis was needed to account for the specifics of the control system design. For this reason, flight control systems were synthesized using CONDUIT (Ref. 12) to a common set of handling qualities-oriented guidelines following a multi-objective function optimization procedure.

The general optimization philosophy was to jointly minimize motor usage and crossover frequency, while primarily enforcing closed-loop robust stability margin and performance constraints—disturbance rejection bandwidth (DRB) (and disturbance rejection peak (DRP)) for the main (i.e., heave, roll, pitch and yaw) control loops and minimum steady state error for the ESC loops. Additionally, constraints to ensure minimum eigenvalue damping and crossover frequency were imposed.

Simple Proportional-Integral (PI) or Proportional-Integral-Differential (PID) feedback compensators were used in all control loops, including the ESC loops. Control loops were configured into a nested loop structure with the ESC closing the loop on the aircraft and motor dynamics, and the heave, roll, pitch and yaw feedback loops closed around this. A fixed control mixing inherited from the NDARC solution was employed to allocate speed commands to the individual ESC units in response to heave, roll, pitch and yaw commands from the outer loops. One ESC loop was configured for each rotor-motor pair, such that N_R loops existed in parallel. All ESC gains were assumed identical for each motor. Thus, only a single set of design parameters needed to be computed. Rotor 1 (the front right rotor) was designated to be the reference rotor, for purposes of the optimization problem setup.

The inner-loop (ESC) gains were optimized simultaneously with the outer-loop feedback gains in a single-pass approach. Stability margins for the ESC loops were computed with the outer loops open, whereas individual outer control loop margins were computed with all other loops closed. This was done by breaking only the designated loop. In order to adequately compare the three different configurations, the control systems needed to be designed to a common set of criteria (Table A1). If the solution failed to meet all hard and soft constraints, the motor current limit was increased, and a new solution was calculated. This process was repeated until all constraints were satisfied.

Feedback Solution

Multiple studies (Ref. 2, 4-6, and 14-17) have shown that ESC bandwidth significantly affects the amount of open-loop phase margins available. For the quadrotor and octocopter configurations of this study, DRB targets were met with satisfactory phase margins (Figure 8). Special attention should be paid to the roll axis solution. While the bare airframe quadrotor was dynamically very similar in roll and pitch, the higher roll DRB specification required higher ESC bandwidth.

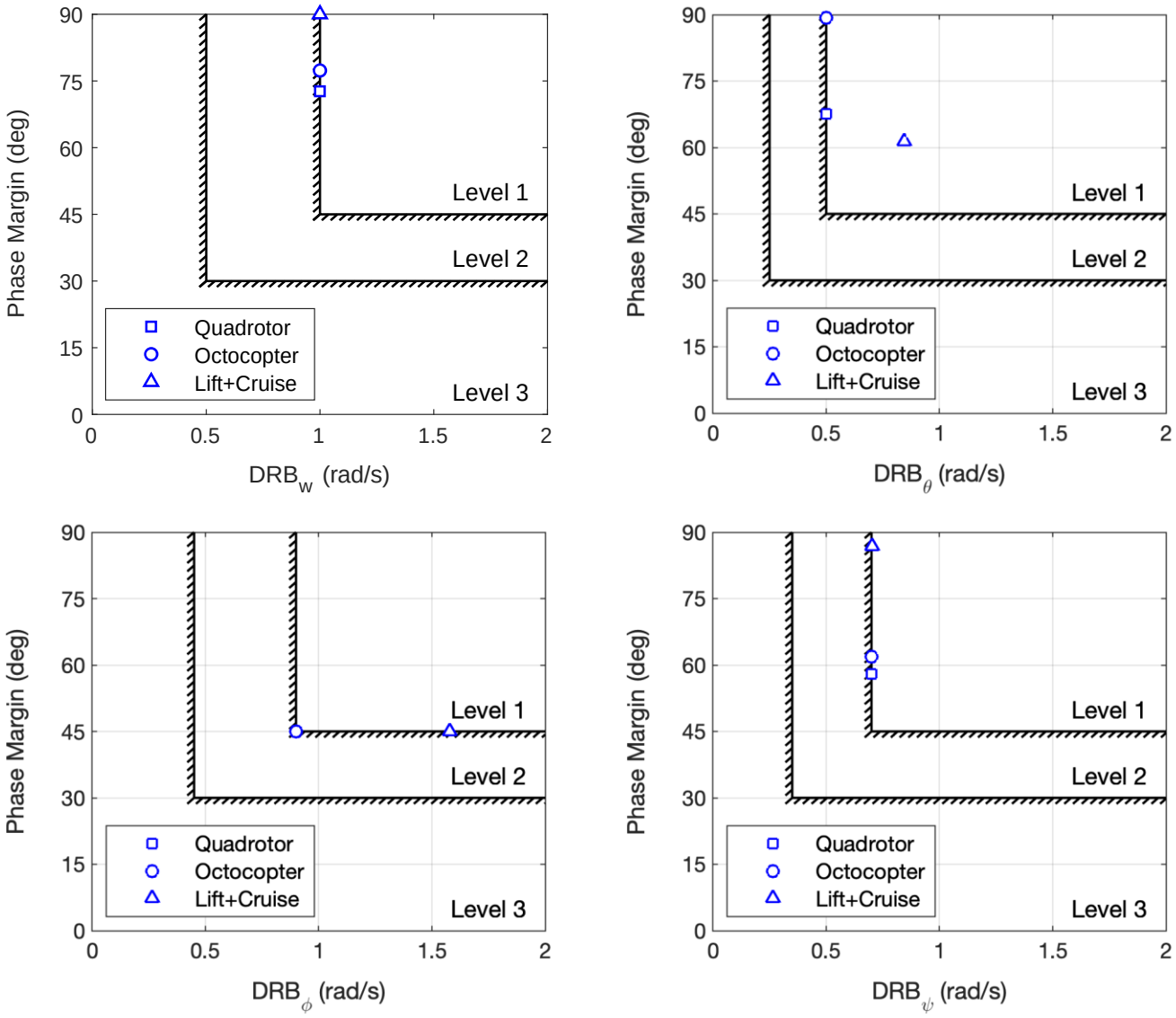

Figure 8. DRB and phase margins.

Optimal ESC bandwidth, characterized in Figure 6 by the motor step response rise time, was the minimum needed to ensure both roll DRB and phase margin requirements were met. There exists a direct correlation between ESC bandwidth and motor usage: increasing one causes the other to increase as well. Hence, the motor usage objective function could only be reduced at the expense of ESC bandwidth. Further reductions in motor usage were not feasible, because a lower ESC bandwidth would have been insufficient to meet the DRB and PM specifications.

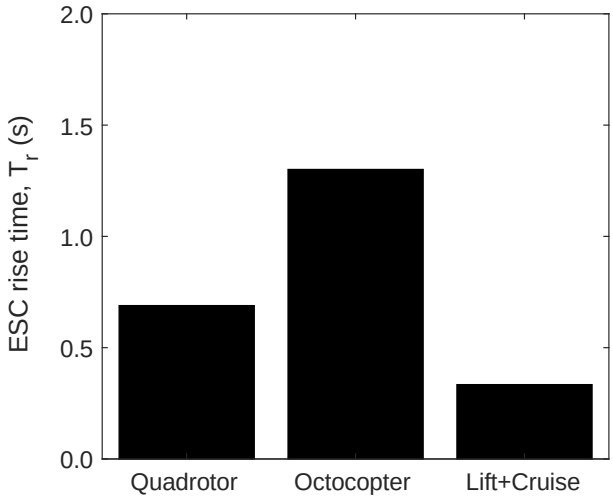

Figure 9. ESC response rise time.

With increased maximum current available, all three vehicle configurations were able to achieve Level 1 handling qualities for the feedback requirements studied. Values for the stability margins, DRB, DRP, damping ratio, and actuator RMS are listed in the Tables 3-5 for each of the axes as well as the ESC rise time for each vehicle configuration. The damping ratio corresponds to the 0.5-4 rad/s frequency range. A solution for the command module was also found through optimizing the CONDUIT process for the quadrotor configuration.

Feedback Analysis

i. Quadrotor

The quadrotor achieved an optimized phase three solution in CONDUIT with a rise time of ~0.69 seconds. DRB was the limiting spec for each of the axes. Heave, yaw, and pitch had additional stability margin, however, roll was limited in the phase direction (~14.3 dB, 45 deg). Heave was, by far, the axis that demanded the most current (as evidenced by the actuator RMS spec, ~1.07) with about twice the magnitude as yaw, the second most demanding axis. Roll followed, and pitch was the least demanding axis for current draw.

Table 3: Quadrotor CONDUIT summary.

	ESC		Heave	Yaw	Pitch	Roll
Phase margin	88.3	Phase margin	72.7	58.0	67.7	45.0
Gain margin	36.2	Gain margin	22.0	23.0	17.1	14.3
Rise time	0.689	DRB	1.00	0.70	0.50	0.90
		DRP	2.23	2.50	2.60	3.92
		Damping Ratio	0.422	0.422	0.422	0.422
		Actuator RMS	1.07	0.474	0.103	0.169

ii. Octocopter

The octocopter converged at a phase 3 solution with tight convergence in CONDUIT with a rise time of ~1.3 seconds. This is the highest rise time of the three configurations studied. Interestingly, this is a much higher value than previously theorized would be necessary to obtain adequate handling qualities, however, all required constraints were achieved with Level 1 specifications. All four axes optimized to the Level 1/2 boundary for DRB. For roll, DRP and stability margin in the direction of phase also reached Level 1/2 boundaries, making roll the limiting axis for the octocopter. This is logical for this particular octocopter configuration which has four rotors aligned on each side of the body. However, the heave is the most demanding axis from an actuator RMS (i.e. current draw) perspective, followed by yaw, roll, and then pitch. This is consistent with the quadrotor configuration described above.

Table 4: Octocopter CONDUIT summary.

	ESC		Heave	Yaw	Pitch	Roll
Phase margin	107.7	Phase margin	77.3	61.8	89.3	45.0
Gain margin	29.0	Gain margin	24.1	25.7	15.8	12.5
Rise time	1.30	DRB	1.00	0.700	0.500	0.900
		DRP	1.18	1.31	2.11	5.00
		Damping Ratio	0.468	0.468	0.468	0.468
		Actuator RMS	0.850	0.486	0.167	0.291

iii. Lift + Cruise

The LPC configuration had an overall rise time of ~0.33 seconds, the lowest of the three configurations studied. Similar to the other two vehicles studied, the heave and yaw optimized to the Level 1/2 boundary for DRB. However, unlike the other two configurations, the pitch axis optimized the Level 1/2 boundary for the damping ratio and minimum cross over frequency spec (2 rad/s). Additionally, the roll axis simultaneously converged to the Level 1/2 boundary for the DRP, damping ratio, and stability specifications in the direction of phase with margin still available for DRB. One potential explanation for the difference between the limiting specifications between the quadrotor/octocopter and LPC may be the high disk loading which could cause the rotor to have difficulty damping out the extra motion in the pitch and roll axes. The damping ratio is the lowest of the three vehicles studied which further supports this hypothesis. Reaching the crossover frequency in the pitch axis before the DRB bandwidth is a fall out of the lower gain margin available compared to the other vehicle configurations.

Table 5: LPC CONDUIT summary.

	ESC		Heave	Yaw	Pitch	Roll
Phase margin	86.9	Phase margin	93.4	86.9	61.4	45.1
Gain margin	21.2	Gain margin	26.9	27.1	9.80	10.2
Rise time	0.33	DRB	1.00	0.702	0.846	1.58
		DRP	0.648	0.634	3.67	5.00
		Damping Ratio	0.350	0.350	0.350	0.350
		Actuator RMS	0.418	0.407	0.0953	0.364

iv. Vehicle Comparison

There are multiple observations that can be made by comparing the CONDUIT results of the three vehicle configurations. Beginning with the ESCs, it is worth noting that the heaviest vehicle, the octocopter, had the highest rotor response rise time, but it also had significantly higher phase margin than the other two configurations and the second highest gain margin. This implies that though it had a high rise time, the ESC for the octocopter was the most stable. As described in Ref. 2 this is likely due to the smaller rotors compared to the quadrotor, but comparing to the LPC also allows the inference that it may also be a function of lower disk loading. Alternatively, the LPC has the fastest rise time, but lowest phase and gain margins. Ref. 2 suggested that minimizing rise time must be balanced with actuator usage to produce the most efficient overall design. This should be considered in context of the stability and actuator usage of the vehicles above. Lastly, comparing the damping ratio shows the rotors of the LPC are the least damped, and rotors of the octocopter are the most damped. This means that the LPC rotors may have a greater tendency to become unstable. This is supported by the lower gain and phase margin for the LPC compared to the other vehicles.

Comparing the heave axis of the three vehicle configurations, shows similar stability values for the octocopter and quadrotor with the octocopter showing slightly more margin. However, the LPC has more margin in the phase direction for heave. DRB, by design, was the same for the three vehicles. DRP was highest for the quadrotor and lowest for the LPC. While, for the ESC, the LPC had the least stability margin, in heave, the LPC had the most stability margin with low DRP. The optimal solution for the octocopter and quadrotor solutions had lower stability margins and higher DRP. However, for this problem, the stability margin could not be increased without pushing the DRB and damping ratio into the Level 2 region. Comparison of the three configurations seems to indicate that rise time is directly proportional to heave actuator usage, which is the most demanding from an actuator perspective for all three vehicles.

It should be noted that the LPC model also has a pusher prop (Ref. 10), which will affect the results of the LPC yaw results. For this study, the pusher prop was not used as a control input as the intent was to focus on the effects of rotor size and disk loading on the vehicle's stability. For the yaw axis, again, the LPC shows a large margin, comparatively to the other configurations studied, in the phase portion of the stability spec with a low DRP and damping ratio. Likewise, the trend holds that yaw actuator usage is high, but not as high as heave, for the vehicles with the highest rise times. Yaw requires the second largest actuator usage in all three vehicles. The stability in the yaw axis also cannot be increased for the LPC without the DRB and damping ratio becoming Level 2 as defined for this optimization.

The LPC has the least stability margin in pitch, while the octocopter has the most. The gain portion of the LPC has less margin than the other two configurations, but is still well within the defined Level 1 handling qualities criteria. The optimization was limited only by the DRB, for the octocopter, but was limited by the DRB and minimum cross over frequency for the quadrotor (which has larger rotors than the octocopter) and the damping ratio and minimum cross over frequency for the LPC (which has a larger disk loading than the octocopter). The quadrotor and LPC required similar actuator RMS (~0.1) to reach the converged solution, while the octocopter, though more stable, demanded ~0.17, possibly due to its larger gross weight. The low damping ratio for the LPC resulted here in a lower stability, higher DRB and DRP in the pitch configuration. Pitch was the least demanding axis for actuator usage for all three vehicle configurations.

In roll, the stability margins of the vehicle configurations do not vary significantly. However, the LPC has a larger DRB and drives the highest actuator usage of the three. The direct relation between low damping and slower rotor roll response can be derived from momentum theory. Thus, it is logical that the LPC would require more actuator usage to achieve the required response. Roll for the LPC configuration required the most intervention in the CONDUIT set up by the author to find an optimized solution.

Overall, it is of interest that the amount of actuator usage by each axis for all three configurations to achieve Level 1 specifications (as defined) remained in the same order. From most demanding to least, these are heave, yaw, roll, and then pitch. The comparison of the three vehicles confirms that number of rotors and disk loading do affect the power needed to control the vehicle and stability margins of the configuration. The octocopter is the most stable configuration in every axis but roll, which is slightly less stable in the gain margin (by 2dB) than the quadrotor. However, the octocopter requires more actuator usage in every axis but heave (compared to the quadrotor) and roll (compared to the LPC). The LPC is more stable in the heave and yaw, which demand the most actuator usage, than the other two vehicles. However, it has a lower damping value which limits the configuration from being more stable in roll and pitch, and has less stability for the ESC.

Command Model

For the quadrotor only, inverse model and command delay low-order equivalent system (LOES) estimates of the broken loop responses (with the ESC loops closed) were computed from the optimal feedback solution. On account of the ESC crossover frequency being on the order of 3–3.5 rad/s, second-order LOES inverse dynamics models were required for the heave, roll and pitch loops. These provided, overall, a much better fit over the frequency range of interest than first-order models. This was not necessary for the yaw loop, likely because of the direct torque application to the airframe inherently produced by a more typical first-order response.

First-order command filters were used to implement rate command height hold (RCHH) and rate command direction hold (RCDH) response types. A first-order filter was added to the pilot input. By itself, the first-order command model had the tendency to introduce high-frequency commands into the engine voltage inputs because of the discontinuous nature of the derivative of the characteristic first-order system response. For instance, large voltage and current spikes would be commanded from unit step or impulse inputs. This tended to manifest itself also in the form of higher frequency content in the engine current PSD functions and therefore on higher values of the engine usage RMS metric. Addition of the filter gave the overall command model second-order characteristics and a much smoother response, and in turn, more sensible engine usage metrics. In common with all filters, these added "envelope protection" filters had the drawback of increasing the response phase delay. The time constant, therefore, needed to be small enough to minimize the added phase delay and conserve command model first-order qualitative behavior, but it also had to be large enough to alleviate high frequency inputs to the ESC.

Optimal heave and yaw control response specifications, as well as the associated torque margins required, are shown in Figure 10. Yaw specifications are from the proposed changes to ADS-33 (Ref. 18) and heave boundaries are from work done on Translational Rate Command systems for STOVL aircraft in hover (Ref. 19) and often employed in the context of shipboard landings. Heave control, again, was found to require significantly (about six times) higher torque margin limits compared to yaw. It was observed, for the quadrotor, that optimal torque margins required for satisfactory heave response (Figure 10), for maximum stick displacement, were only marginally lower than those from Figure 8 for satisfactory disturbance rejection.

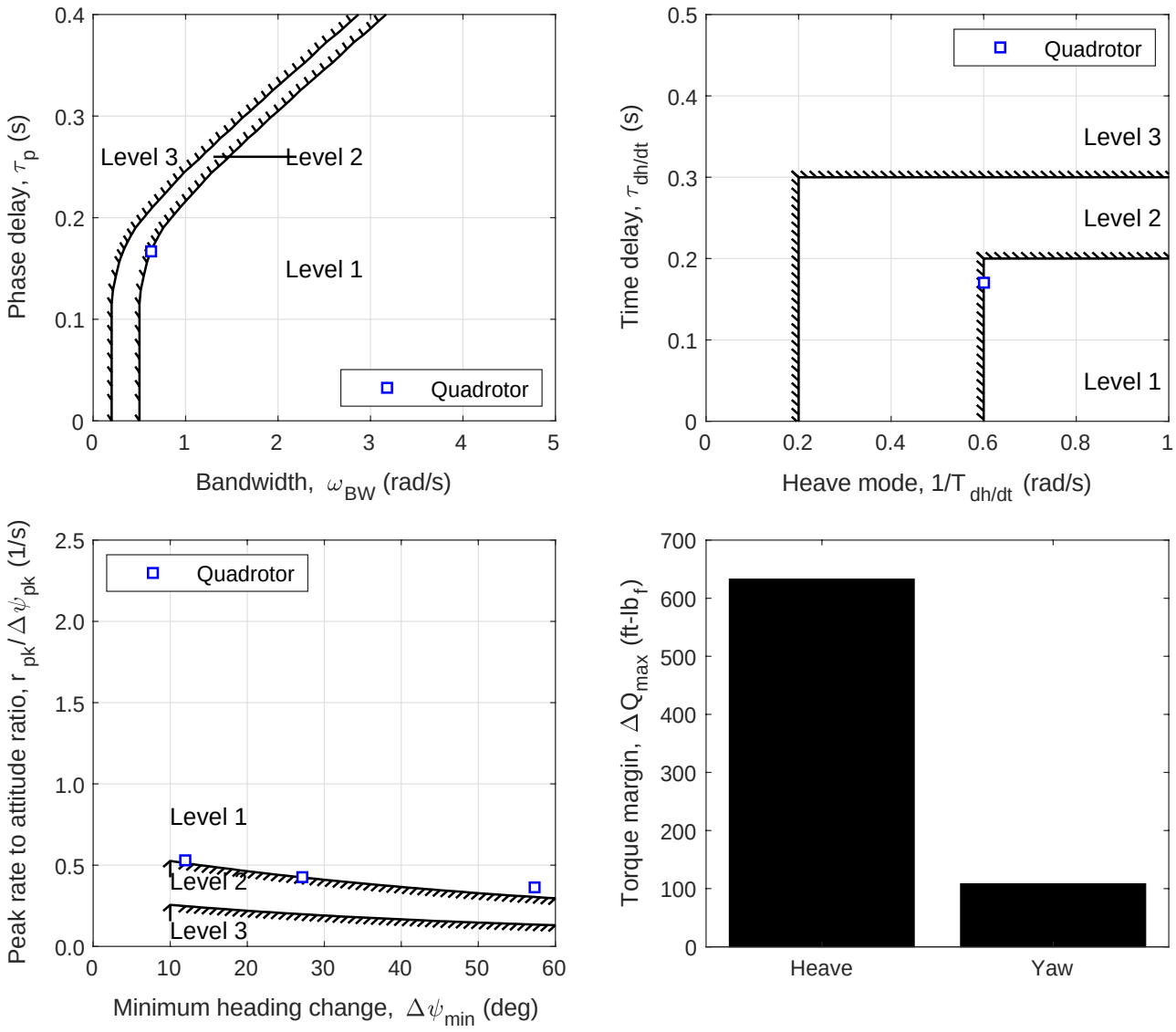

Figure 10: Range of optimal RCHH and RCDH control response specifications and associated propulsion system torque margins.

The remaining defining aspect of the control response requirements is the large-amplitude response of the vehicle which relates to overall control power or agility. For the quadrotor, achievable vertical and yaw rates were about 160 ft/min and 24 deg/s, respectively. Although linear models (such as the ones currently used for conceptual design) are ill-suited to assess overall control power, these results indicate a theoretical capability should the system not be constrained by non-linearities. Architectural limits and other non-linearities are typically ignored.

Design margin optimization results for heave and yaw small-amplitude criteria (shown in Figure 11, Figure 12, and Figure 13) illustrate the strong, directly proportional effect of bandwidth and phase delay on the torque output demands on the propulsion system. Attempts to reduce the heave mode frequency below 0.6 rad/s, resulted in the equivalent time delay increase slightly (up to 0.2 s) and become the new limiting requirement. Note in Figure 11 the overlaid ADS-33 requirement boundaries (in red), for reference. These are significantly less demanding compared to those from Ref. 13, but with these standards, the heave control response handling qualities could ostensibly be Level 1. Further work will be needed to ascertain the appropriate requirements for the UAM mission, however, and the present discussion serves only as a primer to the potential effect on the vehicle design.

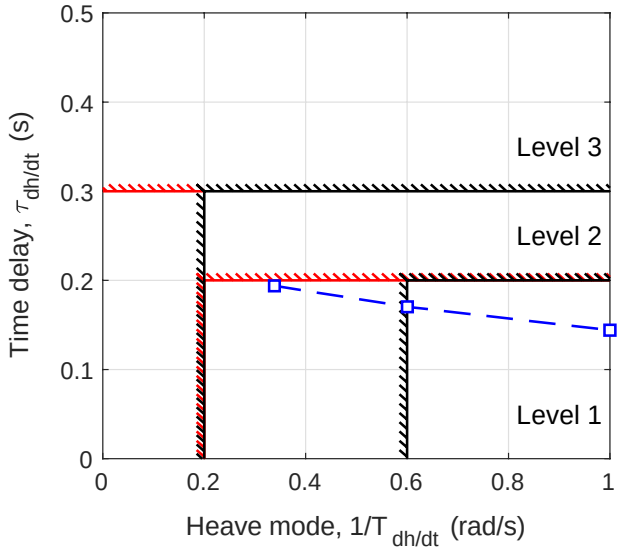

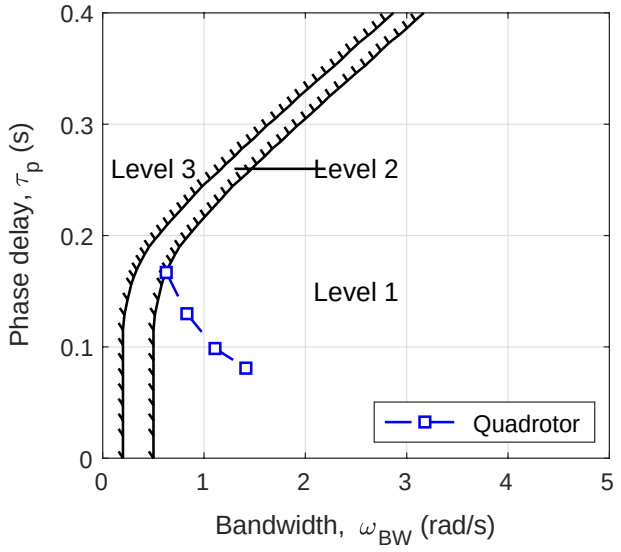

Figure 11. RCHH (with ADS-33 standards overlaid in red) and RCDH control response design margin optimization results.

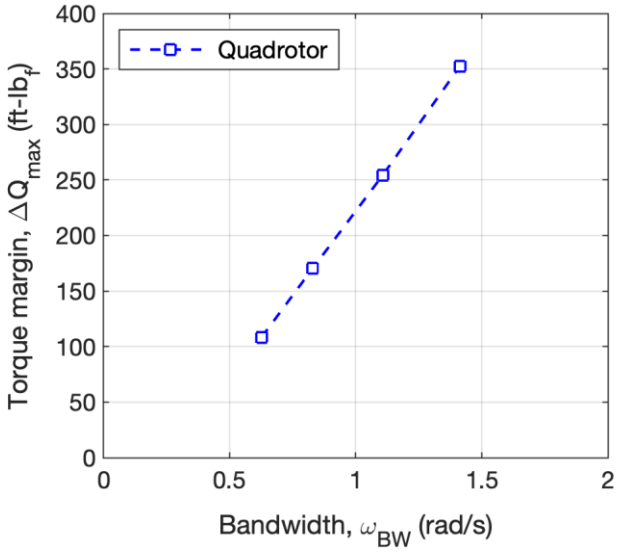

Figure 12. Effect of yaw small-amplitude response criteria on the electric propulsion torque margin required.

Achievable vertical rate was held constant, at about 160 ft/min, throughout the reoptimization. Further reductions in the heave mode frequency were not possible under this constraint, but a 35% reduction in the maximum torque required was obtained. Increasing the heave mode frequency saw, conversely, a reduction in the equivalent time delay but an increase of 80% in the maximum torque margin required (Figure 10).

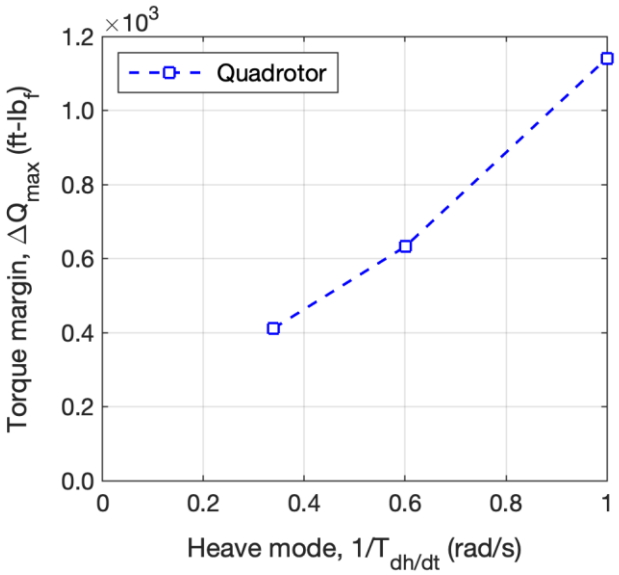

Figure 13. Effect of heave small-amplitude response criteria on the electric propulsion torque margin required.

Similar trends were discernible from the yaw results, where improved handling qualities came at the expense of additional torque margin demands on the propulsion system. For yaw, however, significant improvements (reductions) in the phase delay were also attainable. Small variations in the achievable yaw rates were observed, with values ranging from 22.0 to 23.6 deg/s and averaging about 22.9 deg/s. Along with the bandwidth and phase delay improvements, it was also possible to identify improvements to the moderate-amplitude attitude (i.e., quickness) metrics, in the peak rate to attitude ratio. The penalty, in terms of the maximum torque margins was on the order of a 325% increment, but yet, this was still less than the minimum requirement for heave control.

Finally, the effect of heave control power on the torque margin limits required, as ascertained by the conceptual design linear models, is shown in Figure 14. These results suggest a strong dependency between the vertical agility and the torque margin, with about 4 ft-lb torque required per 1 ft/min of climb rate, for the quadrotor.

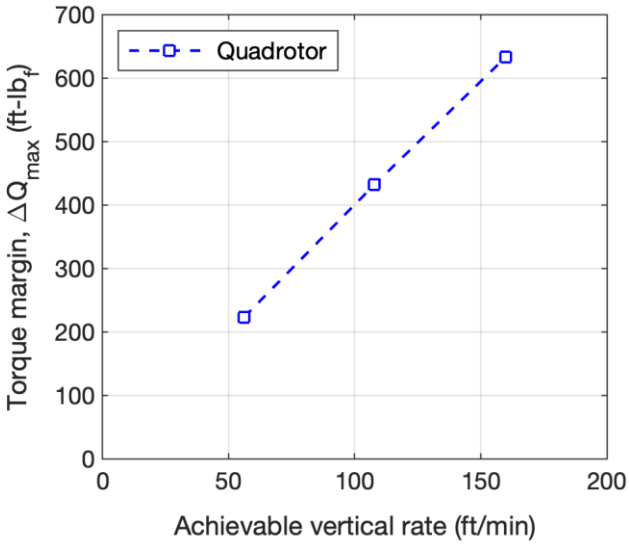

Figure 14. Effect of heave control power on the electric propulsion torque margin required.

POWER AND TORQUE

Because the objective of the study was to determine the theoretical torque and power limits required of the electric propulsion system (to ensure disturbance rejection, robust stability, and control response requirements were met for the vehicle designs), the potential handling qualities effect of actuator rate limiting was not considered at the present time. This will be a crucial, future consideration once a better understanding of the propulsion system limits becomes available. Presently, motor limits, as determined by the motor electrical current were iteratively calculated such that the worst-case motor usage specification was identically 1.0.

The maximum torque margins associated with the motor usage RMS metric for each axis and aircraft model are shown in Figure 13. After the optimal solution was reached, the maximum motor output was calculated such that the engine RMS metrics were scaled to 1.5 (the Level 1/2 HQ limit) exactly:

$$\Delta I_{max} = \frac{\sigma_{eng}}{1.5} (\Delta I_{max})_0 \tag{36}$$

where $(\Delta I_{max})_0$ was the maximum motor current output value for which the RMS metric σ_{eng} was computed and remembering that the relationship between the two is inversely proportional. Conversion from maximum current to torque margin at the shaft followed the relationship:

$$\Delta Q_{max} = r_g K_m \Delta I_{max} \tag{37}$$

In terms of power,

$$\Delta P_{max} = \Omega_{rotor} \Delta Q_{max} \tag{38}$$

These values are dependent on the maximum disturbance input size allowed, which were: 10 ft/s for heave, 10 deg for yaw, and 5 deg for both pitch and roll. Even when considering the maximum torque margin per unit disturbance, results suggested that heave feedback was to place the highest demands on the propulsion system. Incidentally, when scaled relative to the disturbance input size, torque demands required for yaw feedback fell below the requirements for heave, especially for quad and octocopter configurations.

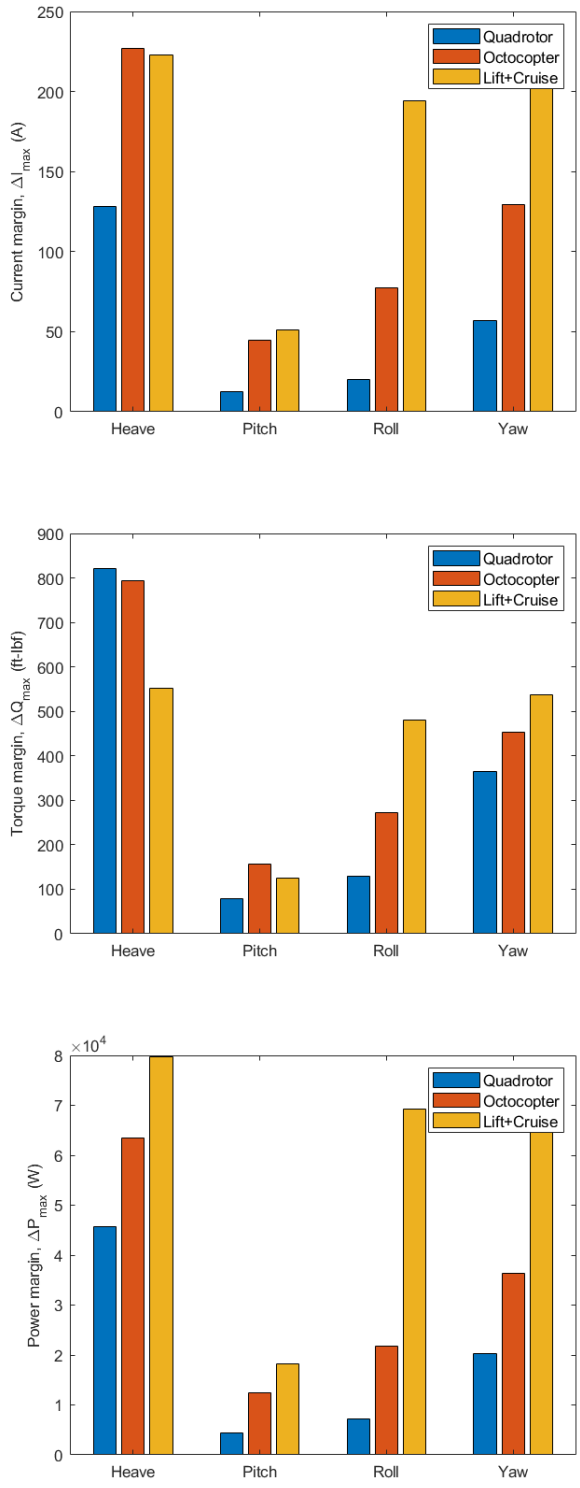

Figure 15: Required current, torque, and power margins.

The magnitude of the power and torque margins required for control emphasizes the challenge and importance of proper motor design for UAM vehicles.

CONCLUSIONS

Three six-passenger reference vehicles sized to the same mission were compared to determine how rotor number and disk loading affected the ability of the vehicle to meet defined Level 1 specifications. All three vehicles met Level 1 specifications when the current was not constrained. The heave axis was the most demanding for all three vehicles, followed by the yaw axis. Required torque and power margins were also the largest for the heave axis in all three configurations. The quadrotor and octocopter were used to assess how the number of rotors affects the motor requirements and the octocopter and a LPC configuration with eight rotors were used to compare the effects of disk loading on motor design. Higher disk loading results in a smaller damping ratio which limited the stability of the LPC vehicle, specifically in pitch and roll. The smaller rotors of the octocopter were more stable than the quadrotor, but the larger octocopter required more actuator usage. Higher rise times (still Level 1) were associated with the vehicles that required more actuator usage in heave and yaw. In this case, the higher actuator usage allowed the vehicles to drive to higher stability solutions. The results of this study emphasize the importance of modeling motor dynamics as part of the control design for all electric, variable speed vehicles.

APPENDIX

Table A1: CONDUIT Specifications.

Feedback Specification	**ESC/Axis**	**Level 1/2 Boundary "Satisfactory"**	**Level 2/3 Boundary "Acceptable"**	**Type of Constraint**
Rise Time	ESC	1.0 second	2.0 seconds	Check only
Low Frequency Gain	ESC	± 0.5 dB	± 3 dB	Hard
Damping Ratio	ESC	0.9	0.8	Soft
Minimum Crossover Frequency	ESC	2.0 rad/s	1.0 rad/s	Check only
Stability Margins	ESC	6 dB, 45 deg	4 dB, 35 deg	Hard
Eigenvalues	All	0	N/A	Hard
Stability Margins	Heave	6 dB, 45 deg	4 dB, 35 deg	Hard
Robust Stability	Heave	±6 dB, ±180 deg ±3 dB, 145 deg	±4 dB, ±180 deg ±2 dB, 155 deg	Hard
Response Comparison	Heave	50 (Total Cost)	100 (Total Cost)	Check only
Disturbance Rejection Bandwidth	Heave	0.5 rad/s	1 rad/s	Soft
Disturbance Rejection Peak	Heave	5 dB	7.5 dB	Soft
Damping Ratio (0.5-4 rps)	Heave	0.15	0.35	Soft
Damping Ratio (4-50 rps)	Heave	0.1	0.2	Check Only
Minimum Crossover Frequency	Heave	0.25 rad/s	0.5 rad/s	Soft
Crossover Frequency	Heave	10 rad/s	15 rad/s	Summed Objective
Actuator RMS	Heave	1.5	2.0	Summed Objective
Stability Margins	Yaw	6 dB, 45 deg	4 dB, 35 deg	Hard
Robust Stability	Yaw	±6 dB, ±180 deg ±3 dB, 145 deg	±4 dB, ±180 deg ±2 dB, 155 deg	Hard
Response Comparison	Yaw	50 (Total Cost)	100 (Total Cost)	Check only
Disturbance Rejection Bandwidth	Yaw	0.35 rad/s	0.7 rad/s	Soft
Disturbance Rejection Peak	Yaw	5 dB	7.5 dB	Soft
Damping Ratio (0.5-4 rps)	Yaw	0.15	0.35	Soft
Damping Ratio (4-50 rps)	Yaw	0.1	0.2	Check Only
Minimum Crossover Frequency	Yaw	0.25 rad/s	0.5 rad/s	Soft

Crossover Frequency	Yaw	10 rad/s	15 rad/s	Summed Objective
Actuator RMS	Yaw	1.5	2.0	Summed Objective
Stability Margins	Pitch	6 dB, 45 deg	4 dB, 35 deg	Hard
Robust Stability	Pitch	±6 dB, ±180 deg ±3 dB, 145 deg	±4 dB, ±180 deg ±2 dB, 155 deg	Hard
Response Comparison	Pitch	50 (Total Cost)	100 (Total Cost)	Check only
Disturbance Rejection Bandwidth	Pitch	0.25 rad/s	0.5 rad/s	Soft
Disturbance Rejection Peak	Pitch	5 dB	7.5 dB	Soft
Damping Ratio (0.5-4 rps)	Pitch	0.15	0.35	Soft
Damping Ratio (4-50 rps)	Pitch	0.1	0.2	Check Only
Minimum Crossover Frequency	Pitch	0.25 rad/s	0.5 rad/s	Soft
Crossover Frequency	Pitch	10 rad/s	15 rad/s	Summed Objective
Actuator RMS	Pitch	1.5	2.0	Summed Objective
Stability Margins	Roll	6 dB, 45 deg	4 dB, 35 deg	Hard
Robust Stability	Roll	±6 dB, ±180 deg ±3 dB, 145 deg	±4 dB, ±180 deg ±2 dB, 155 deg	Hard
Response Comparison	Roll	50 (Total Cost)	100 (Total Cost)	Check only
Disturbance Rejection Bandwidth	Roll	0.5 rad/s	1 rad/s	Soft
Disturbance Rejection Peak	Roll	5 dB	7.5 dB	Soft
Damping Ratio (0.5-4 rps)	Roll	0.15	0.35	Soft
Damping Ratio (4-50 rps)	Roll	0.1	0.2	Check Only
Minimum Crossover Frequency	Roll	1.25 rad/s	2.5 rad/s	Soft
Crossover Frequency	Roll	10 rad/s	15 rad/s	Summed Objective
Actuator RMS	Roll	1.5	2.0	Summed Objective
Command Model				
Rise Time	ESC	1.0 second	2.0 seconds	Check Only
Low Frequency Gain	ESC	±0.5 dB	±3 dB	Check Only
Damping Ratio	ESC	0.9	0.8	Check Only
Minimum Crossover Frequency	ESC	1.0 rad/s	2.0 rad/s	Check Only
Stability Margins	ESC	6 dB, 45 deg	4 dB, 35 deg	Check Only

Heave Response Shipboard Landing	Heave	0.6 rad/s, 0.2 seconds	0.2 rad/s, 0.3 seconds	Soft
Minimum Achievable Vertical Rate	Heave	160 ft/min	55 ft/min	Soft
Actuator RMS	Heave	1.5	2.0	Summed Objective
Yaw Bandwidth	Yaw	Ref. 18	Ref. 18	Soft
Minimum Achievable Yaw Rate	Yaw	22 deg/s	9.5 deg/s	Soft
Quickness	Yaw	Ref. 18	Ref. 18	Soft
Actuator RMS	Yaw	1.5	2.0	Summed Objective

REFERENCES

1. Anonymous, "eVTOL Aircraft Directory," Electric VTOL News, Vertical Flight Society, accessed Apr. 2021. https://evtol.news/aircraft.

2. Withrow-Maser, S., Malpica, C., and Nagami, K., "Multirotor Configuration Trades Informed by Handling Qualities for Urban Air Mobility Applications," Vertical Flight Society 76th Annual Forum Proceedings, Virtual, Oct. 2020.

3. Schuet S., Malpica, C., Lombaerts, T., Kaneshige, J., Withrow-Maser, S., Hardy, G. and Aires, J., "A Modeling Approach for Handling Qualities and Controls Safety Analysis of Electric Air Taxi Vehicles," AIAA Aviation Forum Proceedings, Modeling and Simulation Technologies Conference, June 15–19, 2020.

4. Malpica, C. and Withrow-Maser, S., "Handling Qualities Analysis of Blade Pitch and Rotor Speed Controlled eVTOL Quadrotor Concepts for Urban Air Mobility," Vertical Flight Society International Powered Lift Conference 2020 Proceedings, San Jose, CA, Jan. 21–23, 2020.

5. Walter, A., McKay, M., Niemiec R., Gandhi, F., and Ivler, C., "Hover Handling Qualities of Fixed-Pitch, Variable RPM Quadcopters with Increasing Rotor Diameter," Vertical Flight Society 76th Annual Forum Proceedings, Virtual, Oct. 2020.

6. Bahr, M., McKay, M., Niemiec, R., and Gandhi, F., "Handling Qualities Assessment of Large Variable-RPM Multi-Rotor Aircraft for Urban Air Mobility," Vertical Flight Society 76th Annual Forum Proceedings, Virtual, Oct. 2020.

7. Chen, R. and Hindson, W., "Influence of Dynamic Inflow on the Helicopter Vertical Response," NASA Technical Paper 1431, Jan. 1980.

8. Gareth D. Padfield, "Theoretical Modelling for Helicopter Flight Dynamics: Development and Validation", ICAS-88-6.1.3, Royal Aerospace Establishment, 1988.

9. Houston, Stewart S. "Identification of Factors Influencing Rotorcraft Heave Axis Damping and Control Sensitivity in the Hover, Royal Aircraft Establishment, AE Technical Report 88067, 1989.

10. Silva, C. and Johnson, W., W., Antcliff, K.R., and Patterson, M.D., "VTOL Urban Air Mobility Concept Vehicles for Technology Development," 2018 Aviation Technology, Integration, and Operations Conference, AIAA Aviation Forum, AIAA 2018-3847, Dallas, TX, June 2018.

11. Lawrence, B., Theodore, C. R., Johnson, W., and Berger, T., "A Handling Qualities Analysis Tool for Rotorcraft Conceptual Designs," The Aeronautical Journal, Vol. 122, (1252), June 2018, pp. 960–987.

12. Tischler, M., Colbourne, J., Morel, M., Biezad, D., Levine, W., Moldoveanu, V., "CONDUIT-A New Multidisciplinary Integration Environment for Flight Control Development," NASA Technical Memorandum 112203, USAATCOM Technical Report 97-A-009, June 1997.

13. Franklin, Gene F., Powell, J. David, and Emami-Naeini, Abbas, "Feedback Control of Dynamic Systems," Third Edition. Addison-Wesley, 1994.

14. Walter, A., McKay, M., Niemiec, R., Gandhi, F. and Ivler, C., "Handling Qualities Based Assessment of Scalability for Variable-RPM Electric Multi-Rotor

Aircraft," Vertical Flight Society 75th Annual Forum, Philadelphia, Pennsylvania, May 13-16, 2019.

15. Malpica, C., Withrow-Maser, S., "Handling Qualities Analysis of Blade Pitch and Rotor Speed Controlled eVTOL Quadrotor Concepts for Urban Air Mobility," VFS International Powered Lift Conference 2020, San Jose, CA, Jan. 2020.

16. Niemiec, R., Gandhi, F., Lopez, M. J. S., and Tischler, M. B., "System Identification and Handling Qualities Predictions of an eVTOL Urban Air Mobility Aircraft Using Modern Flight Control Methods ," Vertical Flight Society 76th Annual Forum Proceedings, Virtual, Oct. 2020.

17. Ivler, C., Niemiec, R., Gandhi, F. and, Sanders, F.C., "Multirotor Electric Aerial Vehicle Model Validation with Flight Data: Physics-Based and System Identification Models," Vertical Flight Society 75th Annual Forum, Philadelphia, Pennsylvania, May 13-16, 2019.

18. Chris L. Blanken, Mark B. Tischler, Jeff A. Lusardi, Tom Berger, Christina M. Ivler and Rhys Lehmann, "Proposed Revisions to Aeronautical Design Standard – 33E (ADS-33E-PRF) toward ADS-33F-PRF," Special Report FCDD-AMV-19-01, U.S. Army Combat Capabilities Development Command, Sept. 2019.

19. James A. Franklin and Michael W. Stortz, "Moving Base Simulation Evaluation of Translational Rate Command Systems for STOVL Aircraft in Hover," NASA Technical Memorandum 110399, June 1996.